RSC Advances

ROYAL SOCIETY OF CHEMISTRY

www.rsc.org/advances

Adsorption of Carbon monoxide, Methane and Nitrogen on Alkaline Earth Metal Ion Exchanged Zeolite-X: Structure, Cation Position and Adsorption Relationship

Govind Sethia[a,b], Rajesh S. Somani[a], Hari Chand Bajaj*[a]

[a]Discipline of Inorganic Materials and Catalysis, CSIR - Central Salt & Marine Chemicals Research Institute, Bhavnagar-364 002 (Gujarat), India

[b]Present Address: Center for Catalysis Research and Innovation, University of Ottawa, Biosciences Complex, 30 Marie-Curie, Ottawa, Ontario, Canada K1N 6N5.

*Corresponding author; Email: hcbajaj@csmcri.org

Abstract

Development of zeolite based adsorbents with high adsorption capacity and selectivity is the key requirement for the efficient and economic separation processes. However, less attention has been given so far towards understanding the mechanism of adsorption on the zeolites. In the present study adsorption of carbon monoxide, methane and nitrogen on zeolite-X exchanged with magnesium, calcium, strontium and barium cations was carried out using volumetric gas adsorption method. Calcium, Strontium, and Barium ion exchanged zeolite-X shows increase in carbon monoxide, methane and nitrogen adsorption capacity. Strontium exchanged zeolite-X shows carbon monoxide adsorption capacity of 28.4 molecules/unit cell and calcium exchanged zeolite-X shows methane and nitrogen adsorption capacity of 18.8 and 13.8 molecules/unit cell, respectively at 303 K and 760 mmHg pressure, maximum among the alkaline earth metal ion exchanged zeolite-X samples. However, barium exchanged zeolite-X shows methane/nitrogen selectivity of 1.78, maximum among the studied samples. The initial heat of adsorption for carbon monoxide, methane and nitrogen increases on calcium, strontium and barium ion exchange, and decreases with increase in the size of the cations due to decrease in the electrostatic interactions. However, magnesium exchanged zeolite-X shows decrease in the heat of adsorption. The significant decrease in adsorption capacity and heats of adsorption on magnesium ion exchange is due to the migration of small size magnesium ions inside the sodalite cages (I' and II') and D6R (Site I) from the super cage (Site II, III and III') during activation, where cations are not accessible for adsorption. The change in adsorption capacity, selectivity and heats of adsorption for alkaline earth metal ion exchanged zeolite-X is discussed in terms of the size, location, and effective charges on the extra-framework cations present in the zeolite

cavity and the subsequent electrostatic interactions between the adsorbed molecules and the extra-framework cations.

Keywords: Zeolite-X, Cation exchange, Carbon monoxide, Methane and Nitrogen adsorption.

1. Introduction

Separation of gas mixtures by adsorption is a well-established process technology and during the past few decades there has been extraordinary growth in the development of adsorption-based technologies for the separation of different gas mixtures.[1-7] Adsorption based separation requires accurate data on single and multi-component gas adsorption equilibrium, kinetics and heats of adsorption.[2,6] The separation of CO, and CH_4 from their mixture with N_2 is one of the important industrially significant separation processes.[8,9] The tail gas stream of ammonia plant contain CO (52%), CH_4 (30%), H_2 (4%) and N_2 + Ar (14%) by volume.[10] Carbon monoxide is usually obtained by separation from the synthesis gas mixture, produced during catalytic conversion or partial oxidation of hydrocarbons contains primarily H_2, CH_4 and N_2 as impurities. The recovery of CH_4 from off gases and its separation from nitrogen is also important as methane is one of the major contributors to the global warming with 20 times higher global warming potential than that of CO_2.[11,12] Natural gas consists of mainly CH_4 (80 to 95%) with variable amount of impurities like N_2, CO_2 and other minor impurities like higher hydrocarbons, O_2 and H_2S. For pipeline quality natural gas, the N_2 and CO_2 content should not exceed 4% and 2% respectively.[10] The waste CO, and CH_4 can be used as raw material for fine chemicals synthesis and fuel, if recovered with required purity.

CO, CH_4 and N_2 gas mixtures can be separated by cryogenic separation, liquid absorption or adsorptive separation technologies. The conventional cryogenic separation leaves N_2 as an impurity with CO due to very small difference in the boiling point of CO and N_2 and thus not

suitable for separation. The liquid absorption process, used for the selective absorption and separation of CO from its mixture are commercially available.[13,14] However, the liquid absorption separation suffers from serious drawbacks like high energy requirement for regeneration, corrosion of equipment's, solvent degradation etc. and therefore not suitable for economic large scale separation. Moreover, liquid absorption technology is suitable for only acidic gases like CO, CO_2 etc. and cannot be used for the separation of left over non acidic components like methane, and nitrogen. The adsorption separation technology pressure/vacuum swing adsorption (P/VSA) has the potential for small and large scale economic gas mixture separation, provided with an efficient adsorbent having high adsorption capacity and selectivity.[2,4,15,16] Furthermore, the heat of adsorption for solid adsorbents is generally lower than liquid adsorbents. Consequently, stripping of the adsorbed gases is easier and results in lower energy requirements for regeneration. Adsorption based technologies are thus preferred over liquid absorption based technologies.[17] In view of this, there is a demand for efficient adsorptive separation of CO and CH_4 from different gas mixtures. Many solid adsorbents based on different solids like metal organic frameworks (MOF's), zeolites, aluminophosphate, silica, clay and activated carbons were studied for CO, CH_4, N_2 and H_2 separation from their mixtures.[10,18-27] The equilibrium and dynamic adsorption of CH_4 from its mixture with CO_2, N_2 and H_2 has been reported in various reports.[8,28-33]

The high surface area, pore volume, tunable pore size and high ion exchange capacity are the most commonly used properties of zeolites for adsorptive separation of gases.[1-3,6] The cationic radii, charge, their position and mobility in zeolite cages are the decisive factors for the adsorption of gases, and thus very important for understanding the adsorptive separation of mixtures by zeolites having positively charged exchangeable cations and negatively charged

electron rich framework oxygen atoms. The gases having different physical properties shows different adsorption behavior towards different cation exchanged zeolites.[34]

A detailed knowledge of the adsorption of different gases on zeolite molecular sieve with different extra-framework cations is of great scientific interest.[9,12,33,35-39] The CO, CH_4 and N_2 adsorption on zeolite-X with different extra framework cations has been studied by few researchers.[9,11,12,35-40] and in our previous paper[40] we systematically studied the effect of cesium cation positions on the methane and nitrogen adsorption properties of Zeolite-X. The effect of alkaline earth metal ion exchange on the CO_2 adsorption properties of zeolite-X[41-45], and other zeolites like chabazite[46], beta[47], L[48], and KFI[49] was studied in detail. However, to the best of our knowledge no systematic study for the effect of alkaline earth metal cation exchange on the adsorption of CO, CH_4 and N_2 in zeolite-X was carried out yet. Herein, we carried out the adsorption of CO, CH_4 and N_2 on Ca^{2+}, Mg^{2+}, Sr^{2+} and Ba^{2+} ion exchanged zeolite-X samples at 288, 303, 313 K and 1 atm pressure to develop adsorbents for the selective separation of carbon monoxide and methane from their mixtures with nitrogen. The anomalous adsorption behaviour of magnesium exchanged zeolite-X and the adsorption capacity, selectivity and heats of adsorption for alkaline earth metal ion exchanged zeolite-X samples were studied in relation with the nature and position of Mg^{2+}, Ca^{2+}, Sr^{2+} and Ba^{2+} cations in the Zeolite-X.

2. Material and methods

2.1. Materials

Zeolite-X was procured from Zeochem LLC, Uetikon, Switzerland, and used as received. The salts used for cation exchange include magnesium chloride, calcium chloride, strontium chloride, and barium chloride were purchased from SD Fine-Chem. Limited, India. N_2 (99.999%), CH_4

(99.9%), CO (99.99%) and He (99.999%) from Inox Air Products, India were used for the adsorption isotherm measurements.

2.2. Alkaline Earth Metal Ion Exchange

The alkaline earth metal ions were introduced into the highly crystalline zeolite-X by the conventional cation exchange method. A typical ion exchange involved adding 200 mL of 0.05 M solution of the chloride salt to about 2.5 g of NaX. The solution was heated to 353 K and stirred for 4 h. The solution was decanted and fresh solution was added. This procedure was repeated four times. After the final exchange the solution was vacuum-filtered and washed with copius amount of deionized water until the washings were free from chloride ions as tested with $AgNO_3$ solution. The resulting alkaline-earth metal ion exchanged zeolite samples were dried at 373 K overnight. The percentage of cation exchange was determined by Inductive coupled plasma-optical emission spectrophotometer (ICP-OES) analysis of sodium and cation exchanged zeolite-X. The following terminology is used to describe the ion exchanged samples: the first letter show the exchanged alkaline earth metal cation and the number in brackets shows the percentage of sodium cations exchanged with alkaline earth metal cation for e.g., Mg(70)NaX, shows 70% of the sodium cation present in the zeolite-X were exchanged with the magnesium cations.

2.3. Characterization

X-ray diffraction (XRD) patterns of the materials were obtained using a Philips X'pert MPD system in the 2θ range of 2-60° using CuKα1 (λ = 1.54056 Å). The percent crystallinity of the zeolite samples was determined by considering the intensity of 10 major peaks. Zeolite-NaX was considered as an arbitrary standard for the calculations. The Fourier transform infrared spectroscopy (FT-IR) spectroscopic measurements of alkaline earth metal ion exchanged zeolite-

X were carried out using Perkin-Elmer GX spectrophotometer. The spectra were recorded as KBr pellets of the samples in the wave number range of 400-4000 cm^{-1} with a resolution of 4 cm^{-1}. The surface area and pore volume of the samples were determined from N_2 adsorption data at 77 K. The N_2 adsorption was measured using surface area and pore size analyzer, Model ASAP 2020, (*Micromeritics Inc., USA*) after activating the sample at 623 K overnight under high vacuum. The BET and micropore surface area was determined by BET and t-plot method respectively. The total pore volume was determined from the amount of nitrogen adsorbed at $P/P_o = 0.97$. Microscopic images of alkaline earth metal ion exchanged zeolite-X samples were collected using *LEO 1430 VP* variable pressure scanning electron microscope. An Inductive Coupled Plasma-optical emission spectrophotometer (*ICP-OES, Optima 2000 DV, Perkin-Elmer*) was used to determine the percentage of alkaline earth metal ion exchange, unit cell formula and relative density of prepared samples. For ICP-OES analysis the samples were dissolved in minimum quantity of HF and diluted for less than 10 ppm concentration in solution.

2.4. Adsorption Isotherm Measurements

N_2, CH_4 and CO adsorption isotherms were measured at 288, 303 and 313 K using a static volumetric system (*Micromeritics ASAP 2020).* Before the adsorption measurements, the samples were degassed by heating to 623 K under vacuum (5×10^{-3} mm Hg) for 12 h using degassing system of ASAP 2020. During the adsorption measurements temperature was maintained (± 0.1 K) by circulating water from a constant temperature water bath (*Julabo F25, Germany*). Adsorption capacity, selectivity and isosteric heats of adsorption were determined from the adsorption isotherms measured at 288, 303 and 313 K. The number of gas molecules adsorbed per unit cell of adsorbent was calculated by multiplying the volume of gas adsorbed with a conversion factor (cm^3/g to molecules/unit cell) which was derived by dividing number of

gas molecules adsorbed with total number of unit cells in unit gram of adsorbent. The number of molecules adsorbed and number of unit cells per gram of adsorbent were calculated from ideal gas equation (PV = *n*RT) and molecular weight of adsorbent, respectively.

2.5 Heat of Adsorption and Adsorption Selectivity

The heat of adsorption for CO, CH_4, and N_2 is the measure of their adsorption affinity and strength of interaction with alkaline earth metal ion exchanged zeolite-X. The isosteric heats of adsorption were calculated by using the adsorption data collected at different temperature and Clausius-Clapeyron equation.[50]

$$\Delta_{ad}H^{\circ} = R\left[\frac{\partial lnP}{\partial\left(\frac{1}{T}\right)}\right]_{\theta} \quad (1)$$

Where, $\Delta_{ad}H^{o}$ is heat of adsorption, 'R' is the universal gas constant, 'θ' is the fraction of the adsorbed sites at a pressure '*p*' and temperature 'T'. A plot of ln*p* against 1/T gives a straight line with slope of $\Delta_{ad}H^{\circ}$.

The pure component equilibrium selectivity of two gases A and B was calculated from the adsorption isotherms by using the equation,

$$\alpha_{A/B} = \left[\frac{V_A}{V_B}\right]_{PT} \quad (2)$$

Where, V_A and V_B are the molecules of gas A and B respectively, adsorbed at any given pressure P and temperature T.

3. Results and discussion

CO, CH_4 and N_2 have different molecular properties (Table S1) and the difference in their properties can be utilized for separation of their mixture. CO is acidic while CH_4 and N_2 are neutral in nature and thus basic adsorbents will be required for the selective adsorption of carbon

monoxide. Zeolites are basic in nature with partial negative charge on the framework oxygen atoms generated due to the isomorphic substitution of Si^{4+} by Al^{3+} in the zeolite framework. The basicity of the zeolites can also be increased by exchanging the charge balancing extra-framework cation with cations of higher electro-positivity. Therefore, basic zeolites are characterized by electropositive alkali and alkaline earth cations as extra-framework ions**.**

3.1. X-ray Diffraction

The structure of the zeolite was retained even after repeated alkaline earth metal cation exchange as evident from the retention of all major characteristic peaks of zeolite X. The diffraction patterns indicated that they are highly crystalline, showing reflections in the range of 5-35° which are typical of zeolites (Fig. 1). The observed lattice contraction and phase transformation in strontium exchanged zeolite-X was due to the movement of strontium and sodium ions during the ion exchange.[51] While, the shift of 2 theta values for Ba^{2+} exchanged zeolite-X was due to the exchange of small size sodium cation by lager barium ions in the zeolite cavity.[39] The apparent decrease in crystallinity (Fig. 1) was attributed to the high absorption coefficient of barium ions for CuKα radiation and not because of the structure loss.[52] The Mg(70)NaX, Ca(95)NaX, Sr(95)NaX and Ba(85)NaX samples shows 98, 95, 90, and 68 % crystallinity respectively (Table 1). The percentage crystallinity of the zeolites was determined from the X-ray diffraction pattern by considering the intensity of ten major peaks at 2θ values of 6.15, 10, 15.49, 20.13, 23.38, 26.75, 30.41, 31.05, 32.09, and 33.71.

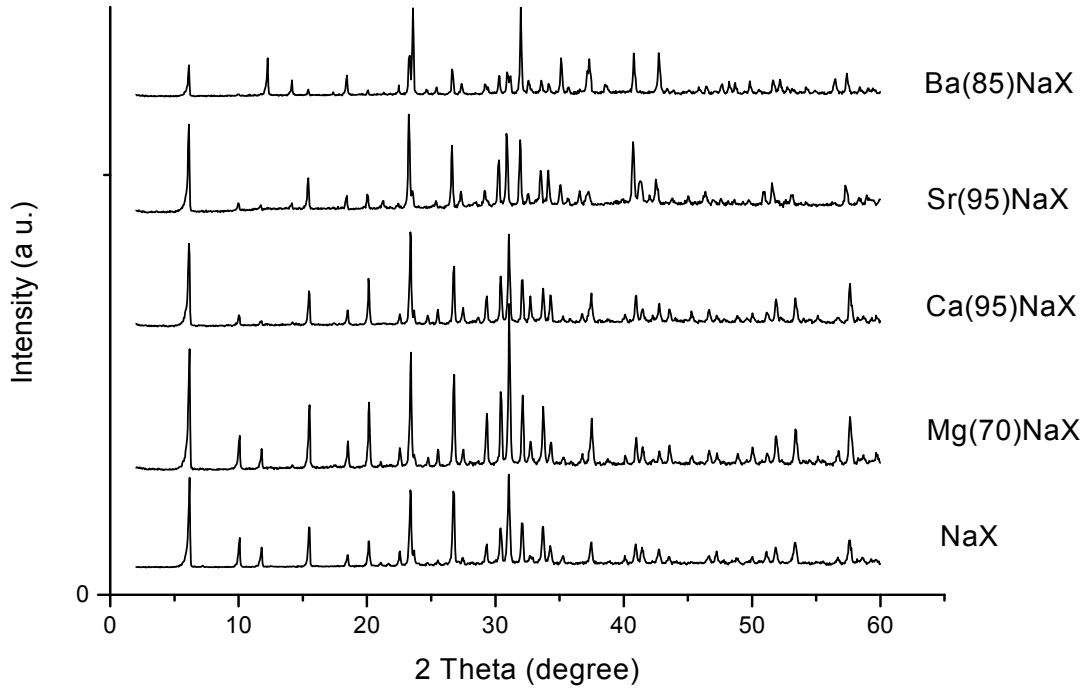

Fig. 1. X-ray powder diffraction pattern of Mg^{2+}, Ca^{2+}, Sr^{2+} and Ba^{2+} cation exchanged zeolite-X.

3.2. Fourier Transform Infrared Spectroscopy

In order to corroborate that the structural framework of zeolite samples was retained after Mg^{2+}, Ca^{2+}, Sr^{2+} and Ba^{2+} ion exchange, FT-IR spectra of the Zeolite-X, Mg(70)NaX, Ca(95)NaX, Sr(95)NaX and Ba(85)NaX was recorded. The infrared spectra (Fig. S1) of alkaline earth metal cation exchanged zeolite showed that the characteristic vibrational bands at 780, 700, 651–570 cm^{-1} of the Faujasite framework are retained with respect to the sodium form of zeolite-X. Therefore, it is concluded that the framework of the zeolite-X remained unaffected after alkaline earth metal ion-exchange.

Table 1. Unit cell composition, relative density, % crystallinity, surface area and pore volume of alkaline earth ion exchanged zeolite-X

Samples	Unit cell formula (anhydrous)	Relative density	(%) Crystallinity	Total Pore volume (cm^3/g)	BET Surface area (m^2/g)	Micropore Surface area (m^2/g)
NaX	$Na_{(88)}Al_{(88)}Si_{(104)}O_{(384)}$	1	100	0.30	692	647
Mg(70)NaX	$Mg_{(31)}Na_{(26)}Al_{(88)}Si_{(104)}O_{(384)}$	0.95	98	0.32	711	675
Ca(95)NaX	$Ca_{(42)}Na_{(4)}Al_{(88)}Si_{(104)}O_{(384)}$	0.98	95	0.31	704	652
Sr(95)NaX	$Sr_{(42)}Na_{(4)}Al_{(88)}Si_{(104)}O_{(384)}$	1.13	90	0.28	622	583
Ba(85)NaX	$Ba_{(38)}Na_{(12)}Al_{(88)}Si_{(104)}O_{(384)}$	1.26	68	0.26	565	530

3.3. Surface Area and Pore volume Measurements

The surface area and pore volume of Mg^{2+}, Ca^{2+}, Sr^{2+} and Ba^{2+} ion exchanged zeolite-X is given in Table 1. Though the crystallinity and structure of ion exchanged samples retained, they differ in textural properties. The surface area and pore volume increases after Mg^{2+}, and Ca^{2+} ion exchange because of the smaller size of Mg^{2+}, and Ca^{2+} ion (Table S2.) and overall decrease in number of cations. The surface area and pore volume for Mg(70)NaX is 711m^2/g and 0.32 cm^3/g respectively, maximum among the studied samples. However, the surface area and pore volume decreases after Sr^{2+} and Ba^{2+} ion exchange due to the comparative large size and high atomic weight of Sr^{2+} and Ba^{2+} ions. Ba(85)NaX shows surface area and pore of 565 m^2/g and 0.26 cm^3/g respectively, minimum among the alkaline earth metal ion exchanged zeolite-X samples. The textural properties of the alkaline earth metal ion exchanged zeolite-X is inversely depends on their density and is in the order of Ba(95)NaX < Sr(85)NaX < NaX < Ca(95)NaX < Mg(70)NaX. The surface area and pore volume of zeolites increases after ion exchange with cations of lower molecular weight, smaller size and higher oxidation state.

3.4. SEM and ICP-OES Analysis

Scanning electron microscopic images shows the octahedral shape of zeolite-X crystals. The SEM also shows no change in the morphology of the zeolite samples even after the Mg^{2+}, Ca^{2+}, Sr^{2+} and Ba^{2+} ion exchange (Fig. S2). The percentage of cation exchange for Mg^{2+}, Ca^{2+}, Sr^{2+} and Ba^{2+} ion exchanged zeolite-X and their corresponding unit cell chemical composition was given in Table 1. Magnesium, calcium, strontium and barium ion exchanged zeolite-X shows 70, 95, 95, and 85 % of ion exchange respectively.

3.5. Adsorption Isotherm and Selectivity

The CO, CH_4 and N_2 adsorption isotherms at 288 and 303 K have been generated and are given in Fig. S3 (a-e) and Fig. 2 (a-e) respectively. The adsorption isotherms are found to be Type I as per the IUPAC classification[1] and clearly shows CO selectivity over CH_4 and N_2, and CH_4 selectivity over N_2 at 288 and 303 K, and 760 mmHg pressure. The equilibrium adsorption capacities of CO, CH_4 and N_2 on Mg^{2+}, Ca^{2+}, Sr^{2+} and Ba^{2+} exchanged zeolite-X has been determined from the adsorption isotherms. The adsorption capacity and selectivity at 303 K and 25, 100 and 760 mmHg pressure is given in Table 2 and 3 respectively. The adsorption capacity increases on alkaline earth metal ion exchange except for Mg^{2+} ion exchange. The adsorption capacity significantly decreases on Mg^{2+} ion exchange and Mg(70)X shows N_2 selectivity over CH_4 in the low pressure region. The anomalous adsorption behavior of Mg^{2+} exchanged zeolite-X is due to very small size of Mg^{2+} ions. Sr(95)NaX shows carbon monoxide adsorption capacity of 28.4 molecules/unit cell and carbon monoxide/methane selectivity of 1.63 at 303 K and 760 mmHg pressure, maximum among the all alkaline earth metal ion exchanged zeolite-X samples. The methane and nitrogen adsorption capacity is in the decreasing order of Ca(95)NaX > Sr(95)NaX > Ba(85)NaX > NaX > Mg(70)NaX. Ca(95)NaX shows highest methane and

nitrogen adsorption capacity. However, Ba(85)NaX shows maximum methane/nitrogen selectivity among the studied samples. The selectivity decreases with increase in partial pressure (Table 4).

Table 2. Adsorption capacities and isosteric heat of adsorption for Mg^{2+}, Ca^{2+}, Sr^{2+} and Ba^{2+} exchanged zeolite-X at 303 K

Sample	Conversion factor	Equilibrium adsorption capacity (molecules/ unit cell)									ΔH° (kJ/mol) at 1 molecule/ unit cell		
		25 mmHg			100 mmHg			760 mmHg					
		CO	CH_4	N_2	CO	CH_4	N_2	CO	CH_4	N_2	CO	CH_4	N_2
NaX	0.5415	1.5	0.5	0.4	5.4	2.3	1.4	15.3	10.1	5.5	26	20	21
Mg(70)NaX	0.5145	5.6	0.6	0.8	6.6	1.8	2.1	10.0	7.9	5.0	17	21	19
Ca(95)NaX	0.5316	12.7	2.9	1.9	18.0	7.7	5.3	24.8	18.8	13.8	33	25	27
Sr(95)NaX	0.6119	6.7	1.4	0.8	14.2	4.7	2.6	28.4	17.4	12	31	22	25
Ba(85)NaX	0.6775	1.5	1.3	0.4	5.2	3.1	1.4	20.8	15.5	8.7	30	22	23

Table 3. Adsorption selectivity for Mg^{2+}, Ca^{2+}, Sr^{2+} and Ba^{2+} exchanged zeolite-X at 303 K

Sample	25 mmHg			100 mmHg			760 mmHg		
	CO/CH_4	CO/N_2	CH_4/N_2	CO/CH_4	CO/N_2	CH_4/N_2	CO/CH_4	CO/N_2	CH_4/N_2
NaX	3.15	4.31	1.37	2.35	3.93	1.67	1.51	2.78	1.84
Mg(70)NaX	9.57	6.94	0.73	3.62	3.16	0.87	1.27	2.00	1.58
Ca(95)NaX	4.36	6.78	1.55	2.34	3.38	1.45	1.32	1.80	1.36
Sr(95)NaX	4.68	8.31	1.78	2.99	5.39	1.80	1.63	2.37	1.45
Ba(85)NaX	1.18	4.28	3.61	1.68	3.67	2.19	1.34	2.39	1.78

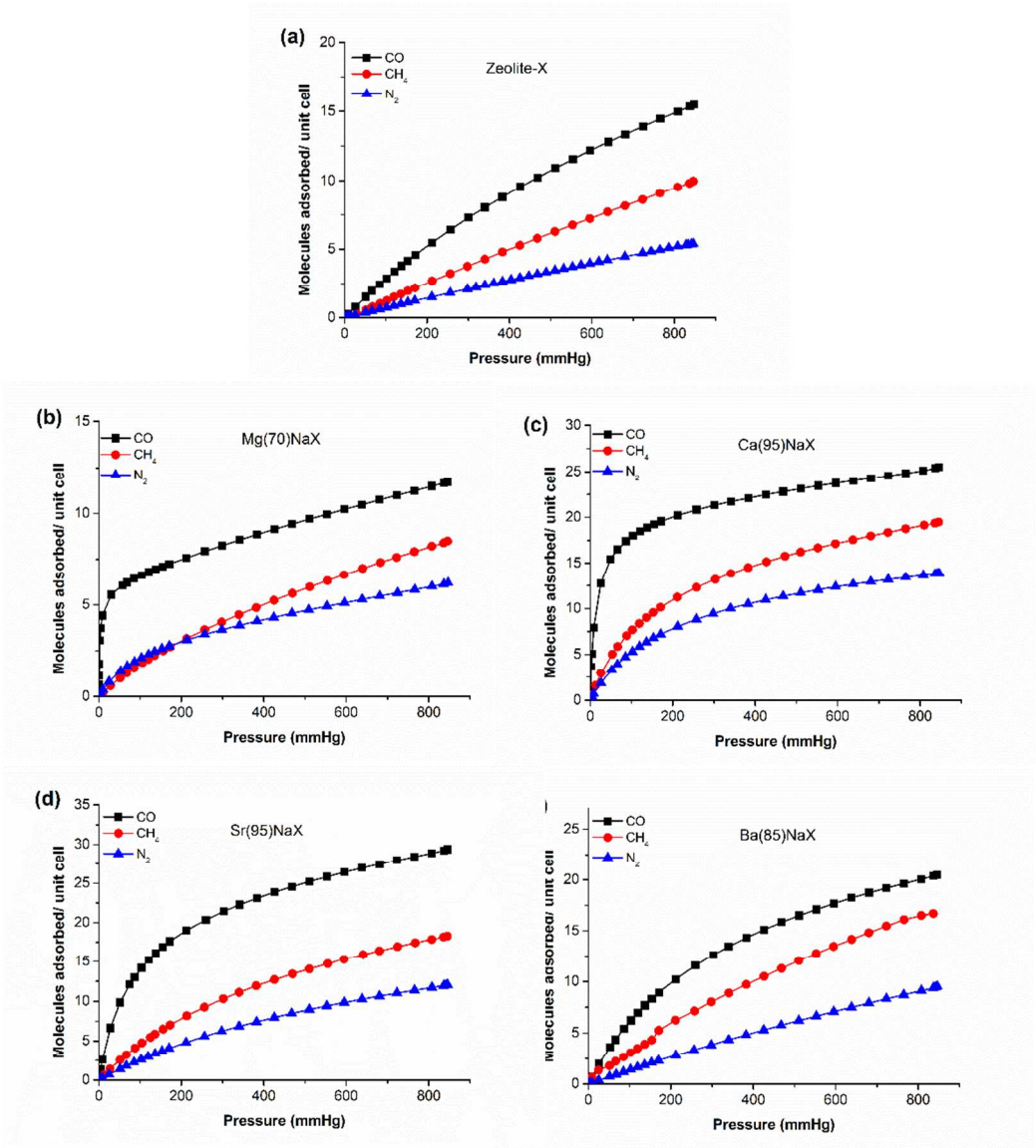

Fig. 2(a-e). Adsorption isotherms of CO, CH_4, and N_2 at 303 K and 760 mmHg pressure (a) Zeolite-X, (b) Mg(70)NaX, (c) Ca(95)NaX, (d) Sr(95)NaX and (e) Ba(85)NaX.

3.6. Structure, Cation Locations and Adsorption in Zeolite-X

The structure of zeolite-X is shown in Fig. 3 Zeolite-X has 88 cations per unit cell which may occupy above six different sites. The detailed discussion about structure and cation positions is given in supporting information. Zeolite-X, Ca(95)NaX, Sr(95)NaX and Ba(85)NaX shows CO adsorption capacity of 15.3, 24.8, 28.4, and 20.8 molecules/unit cell respectively and N_2 adsorption capacity of 5.5, 13.8, 12, 8.7 molecules/unit cell respectively at 303 K and 760 mmHg pressure. Ca(95)NaX shows surface area and pore volume of 704 m^2/g and 0.31 cm^3/g, respectively which are comparable with the surface area (692 m^2/g) and pore volume (0.3 cm^3/g) of parent zeolite NaX. However, Ca(95)NaX shows increase in CO, CH_4, and N_2 adsorption capacity. Mg(70)NaX which also have comparable surface area and pore volume (Table 1) shows significantly low CO, CH_4, and N_2 adsorption capacity. The huge difference in CO, CH_4, and N_2 adsorption capacities for NaX, Mg(70)NaX, and Ca(95)NaX having comparable surface area (± 3%) and pore volume (± 6%), indicates an important role of alkaline earth metal cations with surface area and pore volume in the CO, CH_4, and N_2 adsorption. The major interactions of CO and N_2 with Mg^{2+}, Ca^{2+}, Sr^{2+} and Ba^{2+} exchanged zeolite-X are field gradient quadrupole, field induced dipole and field dipole interactions, which are increases with increasing charge density of cations therefore the CO and N_2 adsorption capacity of Ca^{2+}, Sr^{2+} and Ba^{2+} exchanged zeolite-X is higher than sodium zeolite-X. Mg(70)NaX shows CO, CH_4, N_2 adsorption capacity of 10, 7.9, and 5.0 molecules/unit cell respectively at 303 K and 760 mmHg pressure. Since Mg^{2+} has highest charge density among alkaline earth metal ions, Mg(70)NaX should show high electrostatic interaction potential and higher CO and N_2 adsorption capacity. However, Mg(70)NaX shows adsorption capacity less than Ca^{2+}, Sr^{2+} and Ba^{2+} exchanged zeolite-X. The low adsorption capacity for Mg(70)NaX is because of the migration of Mg^{2+} ions inside β-cages

from the super cages during activation, to minimize their energy and thus the cations unable to effectively interact with gas molecules.[53] Mg^{2+} cation distribution for 72% exchanged dehydrated zeolite-X is 5, 9 and 16 ions at site I, I' and II' respectively with 5, 6 and 15 sodium cations at site I, I', and II, respectively, while for fully Mg^{2+} exchanged zeolite-X it is 14, 4, 24 and 4 at site I, I', II and II', respectively (Table 4). The Mg^{2+} ion distribution show that on increasing Mg^{2+} exchange the number of Mg^{2+} ions in supercage increases, the increased charge density inside β-cages causes repulsion and hence Mg^{2+} ions displaced towards super cage.[53-55] Since Mg^{2+} cations occupy site I, I' and II' which are not exposed to supercage, the ions are unable to interact with the gas molecules and leads to decrease in adsorption capacity. The major part of adsorption capacity of Mg^{2+} exchanged zeolite-X is due to presence of 15 sodium cations at site II. Due to the small size of the Mg^{2+} cations they can sit crystallo-graphically very low in the zeolite cavities, where their electric field is shielded by the surrounding framework oxygen and unable to interact with CO, CH_4 and N_2 molecules.

The cation distribution for dehydrated Ca^{2+} and Sr^{2+} zeolite-X is 16 and 30 ions at site I and II respectively, while Ba^{2+} exchanged zeolite-X has 14.5, 1.5 and 30 ions at site I, I' and II, respectively (Table 4).[54,56-58] Due to presence of 30 cations at site II where gas adsorption occurs, Ca^{2+}, Sr^{2+} and Ba^{2+} exchanged zeolite-X show adsorption capacity higher than zeolite-NaX. The increase in adsorption capacity can be explained by possible shielding of comparative smaller sodium cations by the first few molecules present in a cavity (first shell of gas molecules), which would limit its interaction with other gas molecules. While, larger Ca^{2+}, Sr^{2+} and Ba^{2+} cation experience less shielding and hence able to attract large number of gas molecules in the outer shell. Moreover, CO and N_2 molecules are linear in shape while CH_4 molecule is tetrahedral, the end-on interaction of linear molecule with cation favours additional space to accommodate more

gas molecules around a particular cation in the zeolite cages. The tetrahedral CH_4 molecule could shield the cations for interacting with higher number of molecules and thus the exposure of particular cation located in the cavity could be hindered by the initially adsorbed molecules.

Table 4. Cation positions for Mg^{2+}, Ca^{2+}, Sr^{2+} and Ba^{2+} exchanged zeolite-X

Adsorbent	Number of cation at different sites						Ref.
	I	I'	II	II'	III	III'	
NaX	2.9	21.1+8	31	--	8.6	10.6 + 10.6	Ref.[57,58]
Mg(70) NaX	Mg (5), Na (5)	Mg (9), Na (6)	Na (15)	16	-----	------	Ref.[53-55]
MgX	14	4	24	4	----	-----	
CaX	16	--	30	--	----	-----	Ref.[39,54,55]
SrX	16	--	30	--	----	----	Ref.[39,56]
BaX	14.5	1.5	30	---	---	---	Ref.[39,54]

The CO adsorption follows the order Mg(70)NaX < NaX < Ba(95)NaX < Ca(95)NaX < Sr(85)NaX. Due to polar nature of CO and high charge density of divalent cations the CO molecules comes very close to the small cations and strongly shield them. The strong shielding of small cations by CO molecules decreases their attractive interactions and so they unable to attract large number of molecules. Therefore, the CO adsorption capacity for Ca(95)NaX is less than Sr(85)NaX. N_2 is non polar with polarizability and quadrupole moment less than CO. Therefore, the electrostatic affinity and adsorption capacity for N_2 is less than CO. The adsorption of N_2 molecule is in the order of Mg(70)NaX < NaX < Ba(85)NaX < Sr(95)NaX < Ca(95)NaX. The CO and N_2 adsorption capacity for Ba(95)NaX is less than Ca(95)NaX and Sr(85)NaX due to decrease in surface area, pore volume and low electron density of Ba^{2+} cations. Zeolite-X, Ca(95)NaX, Sr(95)NaX and Ba(85)NaX shows CH_4 adsorption capacity of

10.1, 18.8, 17.4, and 15.5 molecules/unit cell respectively at 303 K and 760 mmHg pressure. CH_4 has neither dipole nor quadrupole moment but high polarizability so field induced dipole interactions dominates. With increasing cation size the polarizing power and pore volume of alkaline earth ion exchanged zeolite-X decreases causing decrease of CH_4 adsorption capacity. At the same time, the shielding of cations by methane molecules decreases with increase in cationic size, therefore, the adsorption capacity of CH_4 for Ca^{2+}, Sr^{2+} and Ba^{2+} zeolite-X is comparable. The adsorption of gases is govern by both textural, and chemical properties of alkaline earth metal cation exchanged zeolite-X and molecular properties of CO, CH_4, and N_2 gas molecules. Therefore, their adsorption capacity and selectivity is the cumulative effect of all properties, with a crucial dominating factor.

The pure component adsorption selectivity at 25, 100 and 760 mmHg equilibrium pressures and 303 K are given in Table 4. The Ca(95)NaX, Sr(95)NaX and Ba(85)NaX shows selectivity higher than sodium zeolite-X in the low pressure region. However, the selectivity decreases with increasing pressure. Among the alkaline earth metal ion exchanged zeolite-X, Mg(70)NaX shows highest CO/CH_4 and CO/N_2 selectivity of 9.6 and 6.9 respectively at 303 K and 25 mmHg pressure. The high CO/CH_4 and CO/N_2 selectivity for Mg(70)NaX at 25 mmHg pressure is because of the high CO adsorption in the low pressure region, due to the high polarizing power Mg^{2+} ions. All alkaline earth metal ion exchanged zeolite-X samples shows CH_4 selectivity over N_2. However, Mg(70)NaX shows N_2 selectivity over CH_4 in the low pressure region ($\leq$ 200 mmHg). The change in selectivity is because of high N_2 adsorption in low pressure due to strong quadruple interactions between N_2 and Mg^{2+} ions having high charge density. Sr(95)NaX shows CO/CH_4 selectivity of 1.63 and , while Ba(85)NaX shows CH_4 /N_2 selectivity of 1.78 at 303 K and 760 mmHg pressure, maximum among the alkaline earth metal ion exchanged zeolite-X.

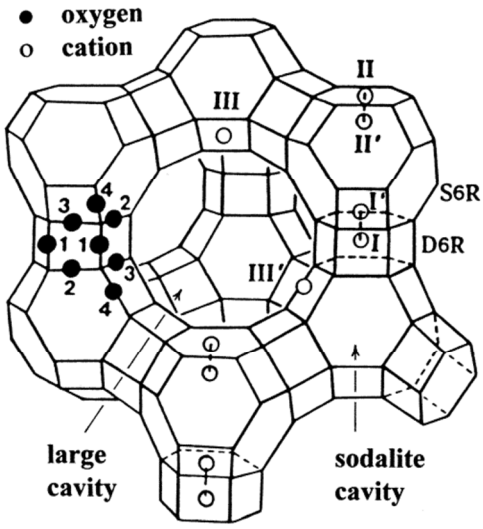

Fig. 3. The framework structure of zeolite-X. Reproduced with permission from ref 10. Copyright 2010 American Chemical Society.

3.7. Heat of Adsorption

The CO, N_2 and CH_4 heats of adsorption at 1 molecules/unit cell for Mg^{2+}, Ca^{2+}, Sr^{2+} and Ba^{2+} ion exchanged zeolite-X are given in Table 2. The isosterric heats of adsorption was calculated using adsorption isotherms data and Clausius-Clapeyron equation. The difference in the adsorption behavior of alkaline earth metal ion exchanged zeolite-X toward CO, N_2 and CH_4 molecules is due to the differences in their interactions with different extra-framework cations. The interactions between zeolite and adsorbed CO, N_2 and CH_4 molecules involve electrostatic, induction, dispersion, and short-range repulsive forces. The electrostatic interaction arises between the dipole and quadrupole moments of adsorbed gas molecules and permanent electric field of the zeolite. The permanent electric field depends on the nature of the extra-framework cations and their location in the zeolite cavity. The heat of adsorption for the CO, N_2 and CH_4 decreases with increase in the size of extra-framework cation and is given by equation 4, 5, and 8

respectively (S. I.). The equation 7, 8, and 9 (S. I.) shows that the dipole, induced dipole and quadrupole interactions decreases with increasing equilibrium distance, consequently with increase in cation radii the charge density and strength of electrostatic interaction between CO, CH_4 and N_2 gas molecules and extra-framework cations decreases. The cations are the preferred adsorption sites and are especially important for interacting with polar, quadrupolar and easily polarizable gas molecules. The cations present in the supercage are easily available to interact with the gas molecules. However, the cations present in the β-cages are hidden and not fully exposed for interaction with the gas molecules.

The heat of adsorption for zeolite-X increases on calcium, strontium and barium cation exchange (Table 2). However magnesium exchanged zeolite-X shows decrease in CO and N_2 heat of adsorption. Ca(95)NaX shows maximum heat of adsorption among the studied samples. The CO, CH_4 and N_2 heat of adsorption for Ca(95)NaX is 33, 25 and 27 kJ/mole respectively. The heats of adsorption for calcium, strontium and barium cation exchanged zeolite-X is in the order of Ca(95)NaX > Sr(95)NaX > Ba(85)NaX > NaX. The heat of adsorption of CO and N_2 is higher than CH_4 and is in the order of CO > N_2 > CH_4 (Table 2). The CO molecule possesses permanent dipole moment, quadrupole moment and polarizability, while N_2 has quadrupole moment and polarizability. Therefore, the CO and N_2 molecules shows strong interaction with high charge density divalent calcium, strontium and barium cation in the zeolite-X. The dominant interaction between the CO and N_2 molecules with extra-framework cations are electrostatic, mainly driven by dipole and quadrupole moment of the gas molecules. In calcium, strontium and barium cation exchanged zeolite-X, CO and N_2 molecules are sitting close to cation at site II, inside the supercage. Therefore, CO and N_2 molecule could be found inside the super cage. Moreover on increasing the cation size the distance between both CO, N_2 molecules

and cations increases. Due to higher quadrupole moment (2.5×10^{-26} esu*cm^2) and polar nature of CO, the heat of adsorption and closeness with cations is higher than N_2 and CH_4. Among the three gases studied, CH_4 has polarizability (26.0×10^{25} cm^3) higher than CO (19.5×10^{25} cm^3) and N_2 (17.6×10^{25} cm^3). Due to high polarizability the polarization contribution towards CH_4 adsorption i.e. induced dipole interaction is high. However, the total heat of adsorption for CH_4 is less than CO and N_2 due to absence of permanent dipole moment and quadrupole moment.

Magnesium exchanged Zeolite-X shows decrease in carbon monoxide and nitrogen heat of adsorption (Table 2). Mg(70)NaX shows carbon monoxide, methane and nitrogen heat of adsorption of 17, 21 and 19 kJ/mole respectively. Interestingly, the heat of adsorption for Mg(70)NaX is in the order CH_4 > N_2 > CO. Magnesium exchanged zeolites-X shows anomalous adsorption behaviour. Though, is not studied in detail. Zhang et al.[59] postulate that decrease in methane and nitrogen adsorption capacity and heat of adsorption for magnesium ion exchanged Zeolite-X is because of the incomplete activation of magnesium ions to form Mg^{2+} during activation since its high charge density.

The significant decrease in carbon monoxide and nitrogen heat of adsorption on magnesium ion exchange is because of decrease in electrostatic interactions between magnesium cation exchanged Zeolite-X and carbon monoxide and nitrogen. In the Mg(70)NaX, the small size magnesium ions occupy beta cages (Sites I', II') and double six membered rings (Site I) where the cations are shielded and cannot effectively interact with carbon monoxide, methane and nitrogen gas molecules, only sodium cations which are present inside the super cage at Site II are available for effective electrostatic interactions. However, no significant change in heat of adsorption for methane is because of significant dispersion interactions between methane and zeolite framework.

4. Conclusions

The adsorption isotherms measurements of CO, CH_4 and N_2 were carried out on zeolite-X exchanged with alkaline earth metal ions. On alkaline earth metal ion exchange the adsorption capacity and initial heat of adsorption for CO, CH_4 and N_2 increases except for magnesium exchanged zeolite-X. Mg(70)NaX shows decrease in adsorption capacity and CO and N_2 heat of adsorption. The anomalous adsorption behaviour of Mg(70)NaX is due to very small ionic radius and migration of Mg^{2+} cations in the sodalite cages and double six membered rings during activation. Among alkaline earth metal ion exchanged zeolite-X the Sr(95)NaX shows maximum CO adsorption capacity and the CO adsorption follows the order Mg(70)NaX < Ba(85)NaX < Ca(95)NaX < Sr(95)NaX. The low CO adsorption capacity for Ba(85)NaX is due to decrease in surface area, and pore volume of Ba(85)NaX because of large size and low electron density of Ba^{2+} cations. However, the CH_4 adsorption capacity for Ca^{2+}, Sr^{2+} and Ba^{2+}exchanged zeolite-X is nearly equal. The adsorption isotherm for alkaline earth metal ion exchanged zeolite-X clearly shows CO selectivity over CH_4 and N_2 which is high in low pressure region and CH_4 selectivity over N_2. However, Mg(70)NaX shows N_2 selectivity over CH_4 in the low pressure region. The CH_4/N_2 selectivity increases with increasing cation size. The initial heats of adsorption for alkaline earth metal exchanged zeolite-X is in the order of Ca(95)NaX > Sr(95)NaX > Ba(85)NaX > NaX. The CO, CH_4 and N_2 heat of adsorption for calcium, strontium and barium ion exchanged zeolite-X samples decreases with increasing cation size. Based on the adsorption capacity, selectivity and calculated heat of adsorption, Sr(95)NaX is the best adsorbent for the carbon monoxide separation from its mixture with methane and nitrogen, and Ba(85)NaX is most suitable adsorbent for methane-nitrogen separation among the studied materials. The results shows that not only the nature of alkaline earth metal cations but the position of cations in the

zeolite-X is also a crucial factor to determine their adsorption behavior towards carbon monoxide, methane and nitrogen.

Acknowledgment

G. S. thanks CSIR, New Delhi, India, for financial assistance in the form of senior research fellowship. Authors wish to thank Dr. Sunil Peter and Dr. Ravikumar Iyyamperumal for the fruitful discussions. The authors also thankful to Analytical Science Discipline of CSMCRI for providing analytical facilities.

Supporting information

Structure of zeolite-X, Adsorption interactions and heat of adsorption, Molecular properties of gas molecules, Polarizability, ionic radii and polarizing power of different alkaline earth metal ions, FT-IR spectra and SEM images of Mg^{2+}, Ca^{2+}, Sr^{2+} and Ba^{2+} ion exchanged zeolite-X, Adsorption isotherm for CO, CH_4, and N_2 at 288 K and 760 mmHg pressure.

5. References

1. D. W. Breck, *Zeolite molecular sieves: structure, chemistry, and use*, Wiley, 1973.
2. R. T. Yang, *Gas Separation by Adsorption Processes*, Imperial College Press, 1997.
3. R. T. Yang, *Adsorbents: Fundamentals and Applications*, Wiley, 2003.
4. J. P. Bushinsky, S. P. Goff, D. M. Nicholas and T. M. Roden, U.S. Patent, 4,836,833, June 6, 1989.
5. H. Ishisaka, G. Nakao, Y. Nishimura and S. Takamoto, U.S. Patent, 4,950,462, August 21, 1990.
6. S. Sircar, *Ind. Eng. Chem. Res.*, 2006, 45, 5435-5448.

7. J. R. Cassata, B. G. Mandelik, P. J. Shires and C. P. VAN Dijk, U.S. Patent, 4,479,925, October 30, 1984.

8. A. Jayaraman, A. J. Hernandez-Maldonado, R. T. Yang, D. Chinn, C. L. Munson and D. H. Mohr, *Chem. Eng. Sci.*, 2004, 59, 2407-2417.

9. D. M. Ruthven, *AIChE Journal*, 1976, 22, 753-759.

10. R. S. Pillai, G. Sethia and R. V. Jasra, *Ind. Eng. Chem. Res.*, 2010, 49, 5816-5825.

11. C. A. Grande, F. V. S. Lopes, A. M. Ribeiro, J. M. Loureiro and A. E. Rodrigues, *Sep. Sci. Technol.*, 2008, 43, 1338-1364.

12. F. V. S. Lopes, C. A. Grande, A. M. Ribeiro, V. t. J. P. Vilar, J. M. Loureiro and A. r. E. Rodrigues, *J. Chem. Eng. Data*, 2009, 55, 184-195.

13. A. L. Kohl and R. Nielsen, *Gas Purification*, Elsevier Science, 1997.

14. D. J. Haase and D. G. Walker, *Chem. Eng. Prog.*, 1974, 70, 74-77.

15. D. M. Ruthven, *Principles of Adsorption and Adsorption Processes*, Wiley, 1984.

16. D. M. Ruthven, S. Farooq and K. S. Knaebel, *Pressure swing adsorption*, VCH Publishers, 1994.

17. C. W. Skarstrom, U.S. Patent, 2,944,627, July, 1960.

18. L. Predescu, F. H. Tezel and S. Chopra, *Adsorption*, 1997, 3, 7-25.

19. J.-H. Park, J.-N. Kim, S.-H. Cho, J.-D. Kim and R. T. Yang, *Chem. Eng. Sci.*, 1998, 53, 3951-3963.

20. G. Sethia, G. P. Dangi, A. L. Jetwani, R. S. Somani, H. C. Bajaj and R. V. Jasra, *Sep. Sci. Technol.*, 2010, 45, 413-420.

21. R. R. Pawar, H. A. Patel, G. Sethia and H. C. Bajaj, *Appl. Clay Sci.*, 2009, 46, 109-113.

22. Q. Jiang, J. Rentschler, G. Sethia, S. Weinman, R. Perrone and K. Liu, *Chem. Eng. J.*, 2013, 230, 380-388.

23. G. Sethia, R. S. Pillai, G. P. Dangi, R. S. Somani, H. C. Bajaj and R. V. Jasra, *Ind. Eng. Chem. Res.*, 2010, 49, 2353-2362.

24. H. Tamon, K. Kitamura and M. Okazaki, *AIChE Journal*, 1996, 42, 422-430.

25. Y.-Y. Huang, *J. Catal.*, 1973, 30, 187-194.

26. K. Munusamy, G. Sethia, D. V. Patil, P. B. Somayajulu Rallapalli, R. S. Somani and H. C. Bajaj, *Chem. Eng. J.*, 2012, 195–196, 359-368.

27. S. Cavenati, C. A. Grande and A. E. Rodrigues, *Sep. Sci. Technol.*, 2005, 40, 2721-2743.

28. A. Jayaraman, R. T. Yang, D. Chinn and C. L. Munson, *Ind. Eng. Chem. Res.*, 2005, 44, 5184-5192.

29. R. V. Jasra, N. V. Choudary and S. G. T. Bhat, *Sep. Sci. Technol.*, 1991, 26, 885-930.

30. S. Sircar, *Ind. Eng. Chem. Res.*, 2002, 41, 1389-1392.

31. Q. Min Wang, D. Shen, M. Bülow, M. Ling Lau, S. Deng, F. R. Fitch, N. O. Lemcoff and J. Semanscin, *Microporous Mesoporous Mater.*, 2002, 55, 217-230.

32. P. J. E. Harlick and F. H. Tezel, *Sep. Sci. Technol.*, 2002, 37, 33-60.

33. P. J. E. Harlick and F. H. Tezel, *Sep. Purif. Technol.*, 2003, 33, 199-210.

34. S. Savitz, A. L. Myers and R. J. Gorte, *Microporous Mesoporous Mater.*, 2000, 37, 33-40.

35. G. Maurin, P. Llewellyn, T. Poyet and B. Kuchta, *J. Phys. Chem. B*, 2004, 109, 125-129.

36. O. Talu, S. Y. Zhang and D. T. Hayhurst, *J. Phys. Chem.* , 1993, 97, 12894-12898.

37. D. Saha and S. Deng, *J. Chem. Eng. Data*, 2009, 54, 2245-2250.

38. F. V. S. Lopes, C. A. Grande, A. M. Ribeiro, J. M. Loureiro, O. Evaggelos, V. Nikolakis and A. E. Rodrigues, *Sep. Sci. Technol.*, 2009, 44, 1045-1073.

39. S. A. Peter, A. S. Moharir and R. V. Jasra, *Ind. Eng. Chem. Res.*, 2010, 49, 7524-7529.

40. G. Sethia, R. S. Somani and H. C. Bajaj, *Ind. Eng. Chem. Res.*, 2014, 53, 6807-6814.

41. R. M. Barrer and R. M. Gibbons, *T. Faraday Soc.*, 1965, 61, 948-961.

42. A. Khelifa, A. Hasnaoui, Z. Derriche and A. Bengueddach, *Ann. Chim. Sci. Matér.*, 2001, 26, 55-66.

43. S. S. Khvoshchev and A. V. Zverev, *J. Colloid Interf. Sci.*, 1991, 144, 571-578.

44. D. Bonenfant, M. KHaroune, P. Niquette, M. Mimeault and R. Hausler, *Sci. Technol. Adv. Mater.*, 2008, 1-7.

45. R. Pillai, PhD Thesis, Bhavnagar University, August 2009.

46. J. Zhang, R. Singh and P. A. Webley, *Microporous Mesoporous Mater.*, 2008, 111, 478-487.

47. S.-T. Yang, J. Kim and W.-S. Ahn, *Microporous Mesoporous Mater.*, 2010, 135, 90-94.

48. G. P. Dangi, M. Kuppusamy, R. S. Somani and H. C. Bajaj, *Indian J. Chem. A* 2012, 51A, 1238-1251.

49. T. Remy, S. A. Peter, L. Van Tendeloo, S. Van der Perre, Y. Lorgouilloux, C. E. A. Kirschhock, J. A. Martens, Y. Xiong, G. V. Baron and J. F. M. Denayer, *Langmuir*, 2014, 30, 2968-2968.

50. G. Sethia, H. A. Patel, R. R. Pawar and H. C. Bajaj, *Appl. Clay Sci.*, 2014, 91–92, 63-69.

51. D. H. Olson and H. S. Sherry, *J. Phys. Chem.*, 1968, 72, 4095-4104.

52. H. S. Sherry, *J. Phys. Chem.*, 1966, 70, 1332-1334.

53. A. Dyer and H. Enamy, *Zeolites*, 1981, 1, 7-10.

54. Y. H. Yeom, S. B. Jang, Y. Kim, S. H. Song and K. Seff, *J. Phys. Chem. B*, 1997, 101, 6914-6920.

55. A. A. Anderson, Y. F. Shepelev and Y. I. Smolin, *Zeolites*, 1990, 10, 32-37.

56. M. J. Kim, M. S. Jeong, Y. Kim and K. Seff, *Microporous Mesoporous Mater.*, 1999, 30, 233-241.

57. L. Zhu and K. Seff, *J. Phys. Chem. B*, 1999, 103, 9512-9518.

58. D. H. Olson, *Zeolites*, 1995, 15, 439-443.

59. S. Y. Zhang, O. Talu and D. T. Hayhurst, *J. Phys. Chem.*, 1991, 95, 1722-1726.

Table and Figure Captions:

Table 1. Unit cell composition, relative density, % crystallinity, surface area and pore volume of alkaline earth ion exchanged zeolite-X

Table 2. Adsorption capacities and isosteric heat of adsorption for Mg^{2+}, Ca^{2+}, Sr^{2+} and Ba^{2+} exchanged zeolite-X at 303 K

Table 3. Adsorption selectivity for Mg^{2+}, Ca^{2+}, Sr^{2+} and Ba^{2+} exchanged zeolite-X at 303 K

Table 4. Cation positions for Mg^{2+}, Ca^{2+}, Sr^{2+} and Ba^{2+} exchanged zeolite-X

Fig. 1 X-ray powder diffraction pattern of Na^{+}, Mg^{2+}, Ca^{2+}, Sr^{2+} and Ba^{2+} cation exchanged zeolite-X.

Fig. 2(a-e) Adsorption isotherms of CO, CH_4, and N_2 at 303 K and 760 mmHg pressure (a) Zeolite-X, (b) Mg(70)NaX, (c) Ca(95)NaX, (d) Sr(95)NaX and (e) Ba(85)NaX.

Fig. 3 The framework structure of zeolite-X. Reproduced with permission from ref 10. Copyright 2010 American Chemical Society.

TABLE OF CONTENT